Research Article | Vol. 32, No. 26 / 16 Dec 2024 / Optics Express 47447
Optics EXPRESS

Experimental analysis and modeling of the penetration depth of uniform and apodized integrated Bragg reflectors

FARAH COMIS,[1,*] MYKYTA SHEVCHENKO,[1,2] MU-CHIEH LO,[1,3] AND ALFONSO RUOCCO[1]

[1]Optical Networks Group, Department of Electronic & Electrical Engineering, University College London, London WC1E 7JE, UK
[2]National Physical Laboratory (NPL), Hampton Road, Teddington, Middlesex TW11 0LW, UK
[3]EFFECT Photonics, 5656 AE Eindhoven, The Netherlands
[*]farah.comis.16@ucl.ac.uk

Abstract: Our proposed method quantifies the penetration depth of integrated Bragg gratings that form on-chip Fabry-Pérot cavities. Through the characterization of the integrated cavities, we evaluate the wavelength-dependent penetration depth by studying its impact on the free spectral range and comparing it with theoretical models, for both uniform and apodized gratings. The analysis of the results is relevant for those who model, fabricate and characterize Bragg reflectors as effective mirrors when the length of the order of the wavelength is needed.

1. Introduction

Integrated Bragg gratings are ubiquitous, finding their main application in optical communication. They are mostly used as filters for wavelength-division multiplexing (WDM) [1]. They are used in lasers as mirrors for distributed Bragg reflector (DBR) [2] and distributed-feedback (DFB) lasers [3]. They also find their application in sensing [4]. Furthermore, they are important components for the dispersion engineering of integrated cavities [5,6]. Integrated Bragg reflectors have enabled the achievement of interesting performances in Fabry-Pérot (FP) microresonators. Taking a closer look at these cavities, there has been rising interest in dispersion-compensating strategies, for instance, integrating a dispersion compensating element in the cavity architecture [5]. Dissipative Kerr solitons (DKSs) in integrated microresonators have been demonstrated using dispersive Bragg reflectors [7]. These light sources are typically required to produce a very short pulse duration, on the order of femtoseconds, for applications in high-precision metrology-grade femtosecond sources and for generating broadband frequency combs spanning frequencies from tens of gigahertz to terahertz. This nonlinear mechanism opens the possibility of increasing the bandwidth of coherent optical communication systems [8,9], to meet the increasing data rate demands. Recently, a nanofabricated FP resonator with a Q−factor of 10^5, composed of two photonic crystal resonators, has successfully demonstrated Kerr-frequency-comb generation [10]. Hence, the widespread adoption of Bragg reflectors in FP microresonators for dispersion compensation has become increasingly relevant.

While Bragg gratings used as reflectors provide a wide range of functionalities, there is an underlying issue in the device physics. When light is reflected by the Bragg reflector, it does not reflect precisely from the point where the grating begins. To address this issue, researchers have examined the concept of the penetration depth, or effective length of the grating, denoted as L_{eff}. This term refers to the virtual shifted interface inside the Bragg reflector that defines the actual reflection point. This concept was analytically described in the context of reflectors with a

#534778 https://doi.org/10.1364/OE.534778
Journal © 2024 Received 8 Jul 2024; revised 2 Oct 2024; accepted 16 Nov 2024; published 13 Dec 2024

Optics EXPRESS

constant perturbation period [11]. The penetration depth influences the free spectral range (FSR) of the cavity, further changing the specifications of the device, such as the repetition rate and the etch depth. Therefore, the cavity cannot be designed properly without quantifying the penetration depth of the gratings forming these cavities, which we present in this work. We also present an extended outlook on apodized gratings, commonly used in dispersion compensation applications.

Recently, researchers have conducted experimental investigations to assess the impact of the penetration depth of Bragg reflectors in microcavities [2], and have measured the penetration depth of Bragg grating reflectors in FP refractometers [12]. Nonetheless, the demonstrations and analyses only looked into bulk platforms. Instead, integrated waveguide Bragg gratings are fabricated in high-index contrast material platforms and are lithography-defined. Therefore, an experimental study to find the penetration depth of integrated Bragg gratings, uniform and apodized, is needed.

In this paper, to the best of our knowledge, for the first time, we present an experimental method for accurately determining the penetration depth of uniform and apodized integrated Bragg gratings. The experimental measurements have shown to align with theoretical models, specifically examining different grating lengths within the wavelength range of interest. This underlines the importance of the study for designing on-chip dispersion-aware components.

2. Apodized and uniform gratings design and modeling

We design a silicon nitride on insulator (SiNOI) FP cavity by placing a waveguide in between two integrated Bragg grating reflectors. Its schematic is shown in Fig. 1(a). The devices were fabricated by CORNERSTONE, offering deep-UV lithography for wafer-scale fabrication [13]. The patterns are processed on a single-side polished SiNOI wafer. The buried silicon dioxide layer is thermally grown and has a thickness of 3 μm, which sits on top of a crystalline silicon substrate. The silicon nitride for the device layer is grown using low pressure chemical vapor deposition (LPCVD), with a thickness of 300 nm ± 15 nm. The pattern is defined on the resist. This is followed by an etching process down to the silicon dioxide layer. The resist is then removed, resulting in SiN strip waveguides. The final step of the process involves silicon dioxide cladding deposition, with approximately 2 μm thickness [14]. Figure 1(b) shows the scanning electron microscope (SEM) image of the fabricated apodized gratings. Each section with a perturbation is part of the quadratic apodization, which is taken into account in the penetration depth model.

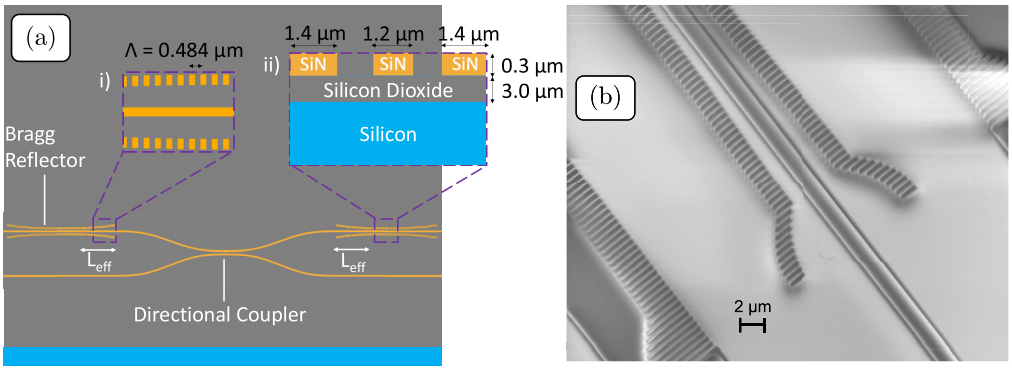

Fig. 1. Device design and fabrication. (a) Schematic of the top view of the Fabry-Pérot cavity with integrated Bragg grating reflectors. i) Bragg corrugation top view, showing its period. ii) The cross-section of the device. (b) Scanning electron microscope (SEM) image of the apodized gratings. (Figures not drawn to scale).

Optics EXPRESS

The forward-propagating light is diffracted backwards by the gratings. This requires the gratings' period to achieve constructive interference at the interface between forward and backward propagating light, ensuring efficient reflection in the backward direction [15]. A wavelength-dependent simulation of the effective index is used for simulating the spectra of the cavities. In our simulations, we account for this dependency to ensure that the simulation and modeling of the wavelength response include the dispersion (hence wavelength-dependent effective index). The period of the grating is expressed in [Eq. (1)]:

$$\Lambda = \frac{\lambda}{2n_{\text{eff}}(\lambda)}\bigg|_{\lambda=\lambda_B}, \tag{1}$$

where λ_B is the Bragg wavelength, n_{eff} is the effective index in the device cross-section, whose dimensions are shown in Fig. 1(a). Therefore, the value of the period, Λ, is calculated to be 0.484 μm at the Bragg wavelength of 1552 nm. The device behaves like a reflector when the Bragg condition is met. Light is coupled into the cavity via a directional coupler that is placed at the center of the cavity.

There is a problem that arises in the design of devices that need to target a specific length, and therefore a specific FSR. These devices are typically designed for applications where precise control over the frequency spacing is essential. These applications include optical frequency comb generation [16], where the precisely-spaced phase coherent frequencies are needed for applications such as optical communication, spectroscopy and metrology [17]. For example, mode-locked lasers are commonly used for optical frequency comb generation [18] since the laser's cavity length determines the repetition rate, corresponding to the FSR.

The penetration depth of the grating, L_{eff}, induces an effective length, which is then non-zero and contributes to the total length of the cavity. Therefore, the FSR is a function of the sum of the physical path, L_{phys}, which represents the separation between the beginning of the two reflectors, and the penetration depth of the reflectors (also known as the effective length of the gratings), L_{eff}. It is important to note that the expression in [Eq. (2)] takes into consideration the wavelength-dependent group index, n_g, of the 300 nm thick SiN waveguide which is intrinsically dispersive [19].

$$\text{FSR} \approx \frac{\lambda^2}{2n_g(\lambda)\left[L_{\text{phys}} + 2L_{\text{eff}}(\lambda)\right]}. \tag{2}$$

The geometrical parameters' effect on the cavity is manifested experimentally: the effective cavity length, measured via the FSR, is different from the cavity's physical length, L_{phys}. Therefore, it is essential to assess the penetration depth of the grating, L_{eff}. The study of the penetration depth of the integrated Bragg gratings is enabled by the use of the designed FP cavities. We also design cavities with different grating lengths with the aim of investigating how the penetration depth of the grating varies as a function of the grating length. This was done for both the uniform and apodized gratings. We simulated, using a finite difference eigenmode (FDE) solver, the effective indices in the C-band for the cross-section shown in Fig. 1(a) ii). The results of the simulation are shown in Fig. 2.

Considering a passive structure with the longitudinally-uniform and apodized Bragg grating under the coupled-wave formalism, the refractive index variation yields [20]:

$$n(z) = n_0 + \mathcal{A}(z) \cdot \Pi\left(\frac{2\pi}{\Lambda} z\right), \quad 0 \le z \le L_{\text{tot}}, \tag{3}$$

where $\Pi(\cdot)$ denotes the periodic Bragg grating shape function, Λ the Bragg grating period, n_0 is the material refractive index, L_{tot} the entire length of the Bragg reflector, and $\mathcal{A}(z)$ the amplitude

Optics EXPRESS

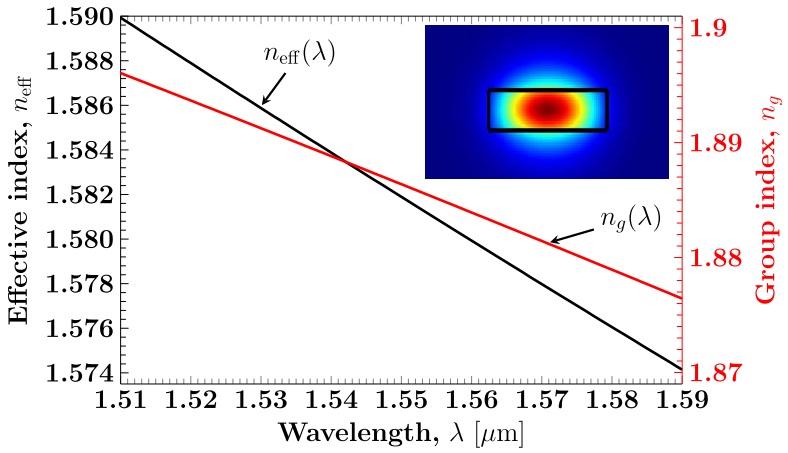

Fig. 2. Effective n_{eff} and group n_g indices (simulated) spectra for a 300 nm SiN film thickness and 1200 nm waveguide width. The inset shows the qualitative mode profile (given in arbitrary unit).

variation of the refractive index modulation, which is defined as:

$$\mathcal{A}(z) = g(z) \cdot \Delta n(\omega), \tag{4}$$

where the apodization function $0 \leq g(z) \leq 1$ is defined as follows:

$$g(z) = \begin{cases} 1 & \text{(uniform-unapodized)} \\ \left(\frac{2z}{L_{\text{tot}}}\right)^2 & \text{(convex-quadratic-apodized)}, \end{cases} \tag{5}$$

and $\Delta n(\omega)$ is the difference between the perturbed and unperturbed waveguides' refractive indices. The electric field distribution along the Bragg grating can be represented as:

$$E(z) = E^+(z)\, \exp\left(-j\frac{\pi}{\Lambda}z\right) + E^-(z)\, \exp\left(j\frac{\pi}{\Lambda}z\right), \tag{6}$$

where $j = \sqrt{-1}$ denotes the imaginary unit, and $E^+(z)$ and $E^-(z)$ are the forward- and backward-propagating components of the electric field, respectively. In order to numerically examine the penetration depth of the integrated Bragg grating, we use the transfer matrix ($\mathbb{T}-$matrix) method [21]. The idea behind this approach is that the Bragg grating structure is divided into N uniform grating segments for which the analytical solution is well-known (see, e.g., [22]). Then, the overall transfer matrix can be obtained as a product of each individual segment's transfer matrix. Applying the boundary conditions and solving the coupled-mode equations, we have the following matrix relation between the electric fields at z and $z + \Delta z$ [23, Ch. 3]:

$$\begin{bmatrix} E^+(z+\Delta z) \\ E^-(z+\Delta z) \end{bmatrix} = \begin{bmatrix} \cosh(\sigma\Delta z) - j\frac{\Delta\beta}{\sigma}\sinh(\sigma\Delta z) & j\frac{\kappa}{\sigma}\sinh(\sigma\Delta z) \\ -j\frac{\kappa}{\sigma}\sinh(\sigma\Delta z) & \cosh(\sigma\Delta z) + j\frac{\Delta\beta}{\sigma}\sinh(\sigma\Delta z) \end{bmatrix} \cdot \begin{bmatrix} E^+(z) \\ E^-(z) \end{bmatrix}, \tag{7}$$

and the initial condition is:

$$\mathbb{T}_0 = \begin{bmatrix} 1 & 0 \\ 0 & 1 \end{bmatrix}, \tag{8}$$

Optics EXPRESS

where $\Delta z = L_{\text{tot}}/N$ is the section length with the number of sections N, β is the propagation constant, κ is the coupling coefficient between forward and backward propagating modes [24], and $\sigma = \sqrt{\kappa^2 - |\Delta\beta|^2}$.

Hence, the connection between two ends of the Bragg reflector is as follows:

$$\begin{bmatrix} E^+(L_{\text{tot}}) \\ E^-(L_{\text{tot}}) \end{bmatrix} = \mathbb{T} \begin{bmatrix} E^+(0) \\ E^-(0) \end{bmatrix}, \tag{9}$$

where the overall $\mathbb{T}-$matrix is the 2×2 matrix with following elements:

$$\mathbb{T} = \mathbb{T}_N \cdot \mathbb{T}_{N-1} \cdot \cdots \cdot \mathbb{T}_k \cdot \cdots \cdot \mathbb{T}_1 = \begin{bmatrix} m_{11} & m_{12} \\ m_{21} & m_{22} \end{bmatrix}, \tag{10}$$

with the matrix $\mathbb{T}_k$ being the transfer-matrix with the coefficients $\kappa = \kappa(k\Delta z)$, $\Delta\beta = \Delta\beta(k\Delta z)$ and $\sigma = \sigma(k\Delta z)$ of the $k^{\text{th}}-$section with $k = \{1, 2, \ldots, N\}$. The complex-valued reflection coefficient is then defined as a ratio:

$$r_E(\omega) \triangleq -\frac{m_{21}}{m_{22}} = |r(\omega)| \cdot \exp[j\varphi(\omega)], \tag{11}$$

with $\varphi = \arg[r_E(\omega)]$ being the phase of the complex reflection coefficient.

The penetration depth for each Bragg reflector is given by [25]:

$$L_{\text{eff}}(\lambda) = \frac{c}{2n_g(\lambda)} \cdot \tau(\lambda), \tag{12}$$

with the wavelength-dependent group refractive index $n_g(\lambda)$ being given by [26]:

$$n_g(\lambda) = n_{\text{eff}}(\lambda) - \lambda \frac{dn_{\text{eff}}(\lambda)}{d\lambda}, \tag{13}$$

and with the wavelength-dependent group delay $\tau(\lambda)$ being defined as [27]:

$$\tau(\lambda) \triangleq \left(\frac{\partial\varphi}{\partial\omega}\right)_{\omega=\omega_B} = -\frac{\lambda_B^2}{2\pi c} \frac{\partial\varphi(\lambda)}{\partial\lambda}. \tag{14}$$

3. Measurement results

We show the method to quantify the penetration depth of the uniform and apodized Bragg reflectors implemented in such high-index contrast platforms. The characterized FP cavities all have a physical length, L_{phys}, of 223 μm. As mentioned in the previous section, we design a set of reflectors with both uniform and apodized gratings. We assume the length of the reflectors to be the same. We measure the transmission spectra of the cavities using a tunable laser (Keysight N777-C) and a power meter (Keysight N7747-C) with a resolution of 0.5 pm. We show the transmission spectra of the FP cavities with both the uniform and apodized gratings in Fig. 3. The response of the cavities is normalized using the transmission spectrum of a straight waveguide located on the same sample. The additional losses can be attributed to several factors, including the particular coupling characteristics of the device, and its symmetric design, which allows for the reflection of some light back to the input. To determine the wavelength-dependent group index, $n_g(\lambda)$, an experimental approach is employed, which involves measuring a reference structure, namely, a ring resonator on the same sample. The measured bandwidth of the cavity featuring uniform gratings is approximately 15 nm. However, in the case of the apodized gratings,

Optics EXPRESS

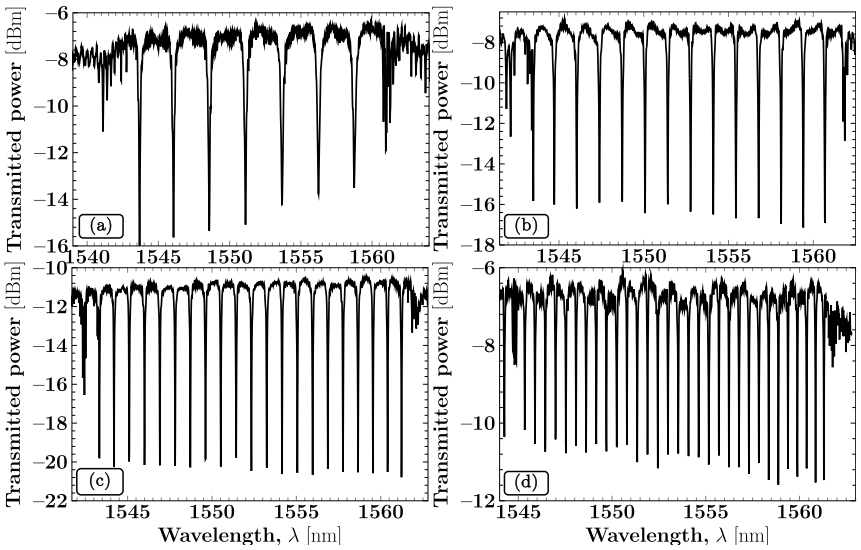

Fig. 3. Spectral response of the Fabry-Pérot (FP) cavity with (a) uniform 1000 μm length gratings, (b) apodized 500 μm, (c) 1000 μm and (d) 2000 μm length gratings on either side.

the bandwidth exhibits a range of variability. This observed variation in bandwidth can be attributed to the variation of the grating strength as a function of grating length.

In Fig. 4, we show the FSR in the wavelength domain for those cavities, which is found by calculating the distance between two adjacent resonance peaks. Subsequently, by utilizing the reference FSR equation in [Eq. (2)], we can calculate the penetration depth of the grating, L_{eff}. In Fig. 4, the FSRs are smaller at the edges of the grating bandwidth following the group delay of the grating, whose absolute value becomes larger in these regions. Instead, at the center of the cavities' bandwidth, the net group delay leads to a pseudo-constant FSR, indicating a near-zero net dispersion cavity, dependent on the grating length.

We compare the results of the uniform and apodized gratings' penetration depths to the transfer matrix ($\mathbb{T}-$matrix) method results. Figures 5(a) and (b) show the wavelength-dependent penetration depth for the uniform and apodized integrated Bragg reflectors, respectively.

With regards to the wavelength dependency of the penetration depth, to account for the intrinsic dispersion of the waveguide used for the cavity, a wavelength-dependent group index, $n_g(\lambda)$, has been taken into account. While for low-index platforms, the wavelength-dependent group index can often be neglected, for high-index contrast platforms like the one used in this work, this becomes a prominent, non-negligible effect to take into account [6].

We exceeded the foundry's minimum feature gap requirement of 250 nm in our design. We design the apodized gratings' minimum gap to be 100 nm, in order to reach the coupling strength for the target bandwidth. We compare the experimental measurements to both the simulation of the ideal device design, whose cross-section shown in Fig. 1(a), and of the device that was fabricated. From the SEM illustrated in Fig. 6, we quantified the widths of the perturbations to be both approximately 1.2 μm. Then, adjacent to both the unperturbed and perturbed waveguides, there is a ridge section, connecting the two. We quantified this ridge section to have a thickness of approximately 0.2 μm. This ridge section is present when the gap between the perturbed and unperturbed waveguides reaches a value below the threshold of 150 nm, confirmed by the SEM. The idealization of the fabricated cross-section is illustrated in the inset in Fig. 6, which provides a comparison with the ideal cross-section, when the gap between the grating and the waveguide reaches a threshold below 150 nm.

Optics EXPRESS

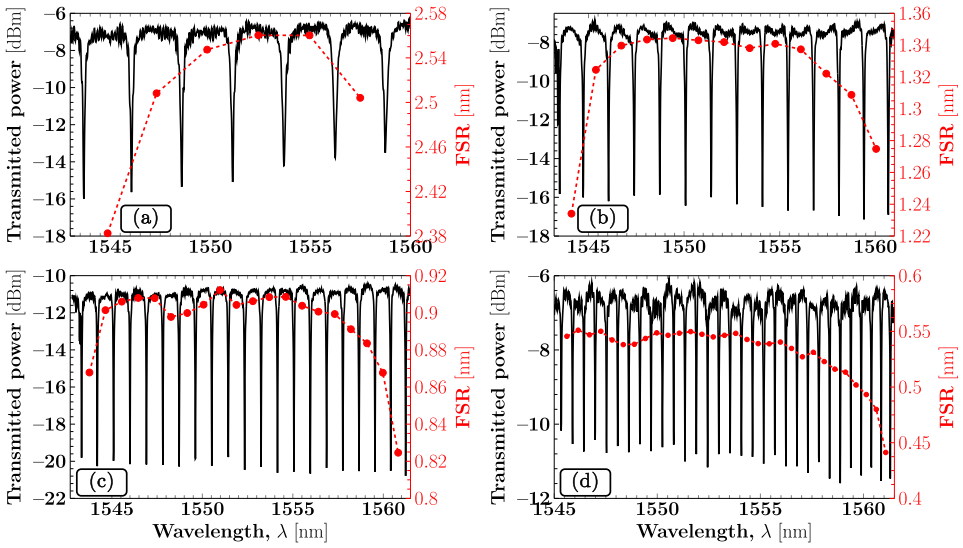

Fig. 4. Experimental free spectral range (FSR) (in red) found from spectral response (in black) of the FP cavity with (a) uniform 1000 μm length gratings, (b) apodized 500 μm, (c) 1000 μm and, (d) 2000 μm length gratings on either side.

Therefore, we simulate the optical properties of the idealization of the fabricated device cross-section. For the uniform 1 mm grating, we measured a penetration depth of approximately 12 μm across the entire bandwidth, as shown in Fig. 5(a). The simulated penetration depth is approximately 4.8 and 8.2 μm for the ideal and fabricated cases, respectively. There is a difference of approximately 31.7% between the fabricated cross-section simulation result and the experimental measurements. Despite the efforts to set the simulation parameters to match the experimental data coming from the SEM, some deviation persists. These variations could be attributed to variations in the fabrication process, contributing to numerical differences in the optical properties. The discrepancy observed between simulation and fabrication highlights the importance of our work, demonstrating that modeling and simulation tools may not consistently replicate devices produced in high-index contrast platforms.

In the case of the apodized gratings, the difference between the ideal and fabricated cross-sections will affect the quadratic apodization of the gratings: this means that after a certain length, the gap between the perturbation and the waveguide will reach a value below the threshold of 150 nm, and the ridge shown in the fabricated cross-section inset in Fig. 6 will be present. We take this into account in the simulation, and we show the results in Fig. 5(b). As seen, the experimentally determined penetration depths of the gratings are in closer agreement with the results of the fabricated cross-section optical properties, with approximately 7.3%, 9.0% and 2.2% deviation on average for the 0.5 mm, 1 mm and 2 mm gratings, respectively.

Furthermore, we investigate the dependence of the penetration depth on the grating length. Figure 7 shows the experimental and simulation results of the penetration depth as a function of the following grating lengths: 1 mm, 2 mm and 4 mm for the uniform gratings, and 0.5 mm, 1 mm and 2 mm for the apodized gratings, at the Bragg wavelength of 1552 nm.

As seen, the theoretical results are in close agreement with the experimental measurements, with approximately 31.7% and 6.0% deviation on average for the uniform and apodized gratings, respectively. The larger mismatch between the modeling and the measurement for the uniform compared to the apodized gratings, can be attributed to the fact that while the uniform grating's design always requires gaps smaller than the foundry's design rules (100 nm), the apodized

Optics EXPRESS

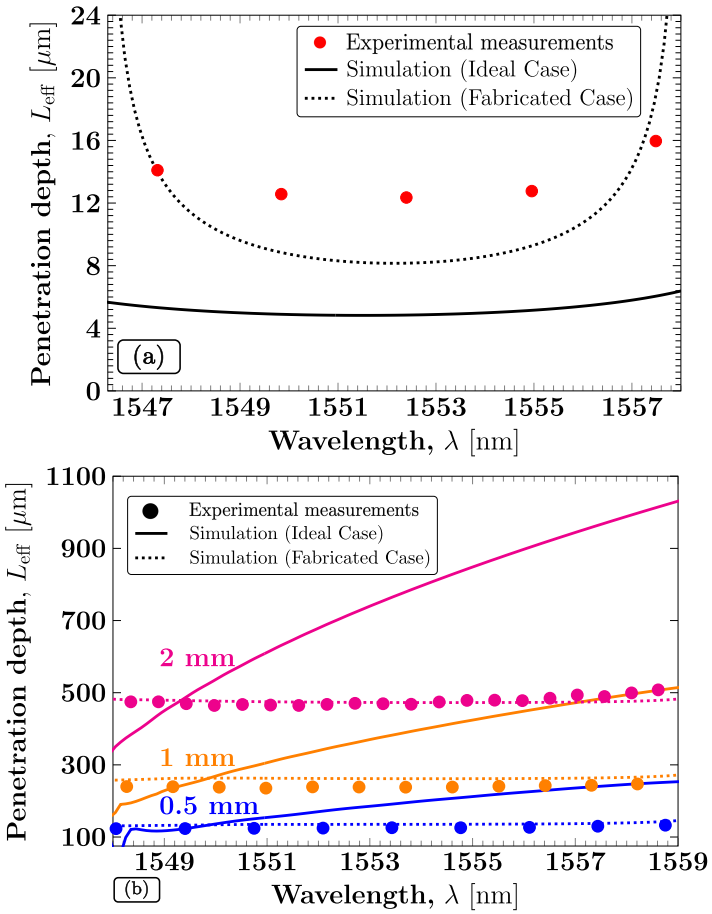

Fig. 5. Penetration depth, L_{eff}, of the 1 mm uniform grating (a) as a function of wavelength; and the (b) 0.5 mm, 1 mm and 2 mm apodized gratings in comparison with theoretical models.

grating's design complies with the foundry's design rules for its initial 15.5%. Therefore, it makes this section's features closer to the one used for the modeling.

In addition, the results also tell us that the penetration depth is constant as a function of the grating length for the uniform gratings. Instead, for the apodized case, the relation is linear. This is justified by the fact that the derivative of the phase of the reflectivity for the uniform case yields a constant, whereas for the apodized case the result of the derivative of the phase of the reflectivity is as a function of the reflector length. The phase is taken as the argument of the reflectivity, which is derived from the coupled-mode equations [11].

Optics EXPRESS

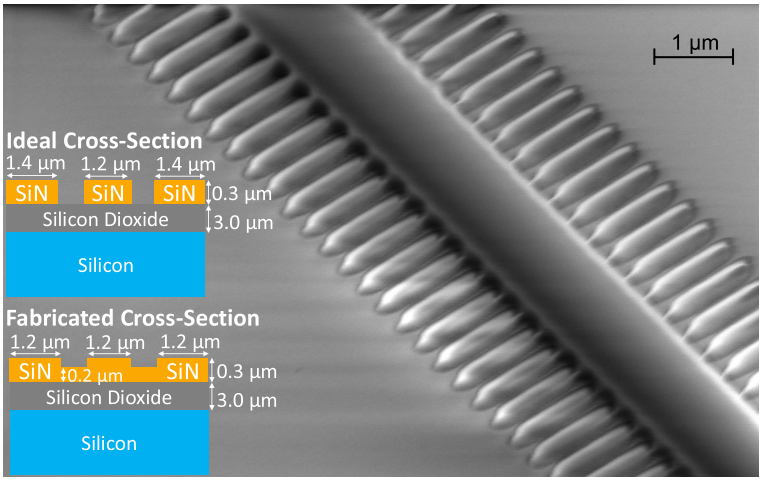

Fig. 6. Scanning electron microscope (SEM) image of the fabricated grating where the gap of the perturbation is 100 nm. Inset shows the ideal and idealization of the fabricated cross-sections (not drawn to scale).

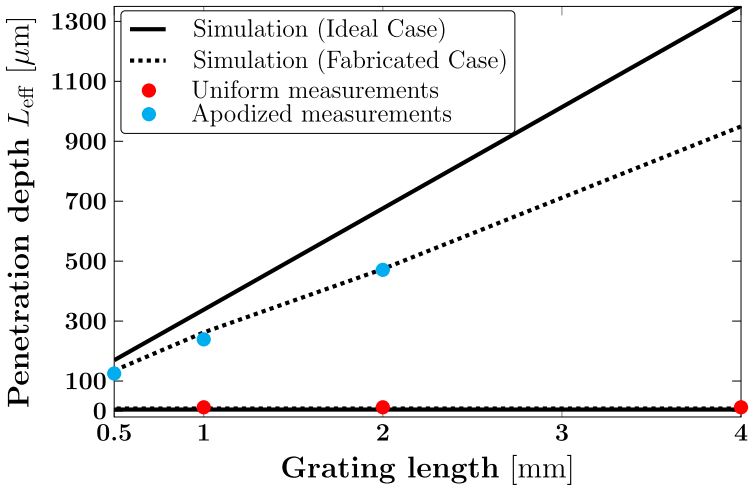

Fig. 7. Penetration depth of uniform and apodized Bragg reflectors as a function of the grating length at the Bragg wavelength of 1552 nm.

Optics EXPRESS

4. Conclusion

In the present work, we have proposed and demonstrated a reliable method to quantify the penetration depth of both uniform and apodized integrated Bragg reflectors implemented in a high-index contrast platform (SiNOI). The set of devices required for the method consists of FP cavities where the reflection is realized with integrated Bragg gratings. The devices have been fabricated using deep-UV lithography under the Cornerstone program [13], based on our design and simulations.

By deploying our method on the FP cavities composed of gratings with different lengths, we have quantified the wavelength-dependent penetration depths of the integrated Bragg gratings, which agree with our theoretical predictions. Despite the efforts to set the simulation parameters to match the experimental data coming from the fabricated device's SEM, the results are consistent with our theoretical results. This is the first demonstration of such a method for dispersive integrated platforms.

Our work represents the first successful experimental analysis for quantifying the penetration depth of integrated Bragg gratings on dispersive integrated platforms. This achievement has significant potential for future advancements in the design of dispersion-engineered cavities.

Funding. CORNERSTONE 2 (EP/T019697/1); Engineering and Physical Sciences Research Council (EP/S022139/1).

Acknowledgments. The authors would like to acknowledge the Engineering and Physical Sciences Research Council (EPSRC) for financial support (No. EP/S022139/1) as well as CORNERSTONE 2 (No. EP/T019697/1) for the fabrication of the devices. Nazca Design was used to generate the mask layout in this work.

Disclosures. The authors declare no conflicts of interest.

Data availability. Data underlying the results presented in this paper are not publicly available at this time but may be obtained from the authors upon reasonable request.

References

1. R. Cheng and L. Chrostowski, "Spectral design of silicon integrated Bragg gratings: A tutorial," J. Lightwave Technol. **39**(3), 712–729 (2021).
2. C. Koks and M. P. van Exter, "Microcavity resonance condition, quality factor, and mode volume are determined by different penetration depths," Opt. Express **29**(5), 6879–6889 (2021).
3. L. Mahler, A. Tredicucci, F. Beltram, *et al.*, "Quasi-periodic distributed feedback laser," Nat. Photonics **4**(3), 165–169 (2010).
4. D. Runde, S. Brunken, C. E. Rüter, *et al.*, "Integrated optical electric field sensor based on a Bragg grating in lithium niobate," Appl. Phys. B: Lasers Opt. **86**(1), 91–95 (2007).
5. K. Shtyrkova, P. T. Callahan, N. Li, *et al.*, "Integrated cmos-compatible Q-switched mode-locked lasers at 1900 nm with an on-chip artificial saturable absorber," Opt. Express **27**(3), 3542–3556 (2019).
6. E. Sahin, K. J. A. Ooi, C. E. Png, *et al.*, "Large, scalable dispersion engineering using cladding-modulated Bragg gratings on a silicon chip," Appl. Phys. Lett. **110**(16), 161113 (2017).
7. T. Wildi, M. A. Gaafar, T. Voumard, *et al.*, "Dissipative kerr solitons in integrated fabry–perot microresonators," Optica **10**(6), 650–656 (2023).
8. B. J. Puttnam, R. S. Luüs, G. Rademacher, *et al.*, "0.61 Pb/s S, C, and L-band transmission in a 125μm diameter 4-core fiber using a single wideband comb source," J. Lightwave Technol. **39**(4), 1027–1032 (2021).
9. J. Pfeifle, V. Brasch, M. Lauermann, *et al.*, "Coherent terabit communications with microresonator Kerr frequency combs," Nat. Photonics **8**(5), 375–380 (2014).
10. S. P. Yu, H. Jung, T. C. Briles, *et al.*, "Photonic-crystal-reflector nanoresonators for Kerr-frequency combs," ACS Photonics **6**(8), 2083–2089 (2019).
11. L. Brovelli and U. Keller, "Simple analytical expressions for the reflectivity and the penetration depth of a Bragg mirror between arbitrary media," Opt. Commun. **116**(4-6), 343–350 (1995).
12. I. Silander, J. Zakrisson, V. S. de Oliveira, *et al.*, "In situ determination of the penetration depth of mirrors in Fabry-P erot refractometers and its influence on assessment of refractivity and pressure," Opt. Express **30**(14), 25891–25906 (2022).
13. "Cornerstone project," https://www.cornerstone.sotonfab.co.uk (2024).
14. "Cornerstone design guidelines," https://www.cornerstone.sotonfab.co.uk/wp-content/uploads/2024/05/cornerstone-silicon-nitride-mpw-8-design-rules.pdf (2024).
15. W. H. Bragg and W. L. Bragg, "The reflection of x-rays by crystals," Proc. R. Soc. Lond. A **88**(605), 428–438 (1913).
16. T. Herr, V. Brasch, J. D. Jost, *et al.*, "Temporal solitons in optical microresonators," Nat. Photonics **8**(2), 145–152 (2014).

Optics EXPRESS

17. R. Sohanpal, H. Ren, L. Shen, *et al.*, "All-fibre heterogeneously-integrated frequency comb generation using silicon core fibre," Nat. Commun. **13**(1), 3992 (2022).
18. J. Rauschenberger, T. M. Fortier, D. J. Jones, *et al.*, "Control of the frequency comb from a mode-locked erbium-doped fiber laser," Opt. Express **10**(24), 1404–1410 (2002).
19. J. Liu, G. Huang, R. N. Wang, *et al.*, "High-yield, wafer-scale fabrication of ultralow-loss, dispersion-engineered silicon nitride photonic circuits," Nat. Commun. **12**(1), 2236 (2021).
20. T. Erdogan, "Fiber grating spectra," J. Lightwave Technol. **15**(8), 1277–1294 (1997).
21. M. Yamada and K. Sakuda, "Analysis of almost-periodic distributed feedback slab waveguides via a fundamental matrix approach," Appl. Opt. **26**(16), 3474–3478 (1987).
22. A. Yariv and P. Yeh, *Photonics: optical electronics in modern communications* (Oxford University Press, 2007).
23. A. Cusano, A. Cutolo, and J. Albert, *Fiber Bragg grating sensors: recent advancements, industrial applications and market exploitation* (Bentham Science Publishers, 2011).
24. T. E. Murphy, "Design, fabrication and measurement of integrated bragg grating optical filters," Ph.D. thesis, Massachusetts Institute of Technology (2001).
25. Y. O. Barmenkov, D. Zalvidea, S. Torres-Peiró, *et al.*, "Effective length of short Fabry-Perot cavity formed by uniform fiber Bragg gratings," Opt. Express **14**(14), 6394–6399 (2006).
26. W. Bogaerts, P. De Heyn, T. Van Vaerenbergh, *et al.*, "Silicon microring resonators," Laser Photonics Rev. **6**(1), 47–73 (2012).
27. A. Pospori and D. J. Webb, "Stress sensitivity analysis of optical fiber Bragg grating-based Fabry–Pérot interferometric sensors," J. Lightwave Technol. **35**(13), 2654–2659 (2017).